

AUTOENCODING FOR THE 'GOOD DICTIONARY' OF EIGEN PAIRS OF THE KOOPMAN OPERATOR

NERANJAKA JAYARATHNE AND ERIK M. BOLLT

ABSTRACT. Reduced order modelling relies on representing complex dynamical systems using simplified modes, which can be achieved through Koopman operator analysis. However, computing Koopman eigen pairs for high-dimensional observable data can be inefficient. This paper proposes using deep autoencoders, a type of deep learning technique, to perform non-linear geometric transformations on raw data before computing Koopman eigen vectors. The encoded data produced by the deep autoencoder is diffeomorphic to a manifold of the dynamical system, and has a significantly lower dimension than the raw data. To handle high-dimensional time series data, Takens's time delay embedding is presented as a pre-processing technique. The paper concludes by presenting examples of these techniques in action.

1. INTRODUCTION

With the rapid advancement of computing machinery scientists acquired capability to analyse large data sets and extract information. Data driven techniques gathered momentum with this recent growth. The modern discipline of data driven sciences can be viewed as a combined outcome of available advanced mathematical techniques and high performance computing. According to [18] data driven discovery is revolutionizing the modeling, prediction and control in a diverse range of complex systems found in turbulence, the brain, climate, epidemiology, finance, robotics, and autonomy.

As opposed to analysing the behaviors of complex dynamical systems in terms of examining single trajectories, it has become possible to empirically discuss global questions in terms of evolution of density [15]. Apart from the traditional analysis using geometrical techniques we can analyse the evolution of dynamical systems using the *Frobenius-Perron* transfer operator [15]. The left-adjoint of the *Frobenius-Perron* operator is the *Koopman* operator. *Koopman* operator produces the values produced by a measurement function applied to the dynamical system. Instead of producing the value of the measurement it produces a value in future.

The data oriented *Koopman* operator analysis perspective for analyzing dynamical systems has become extensively popular and relevant lately in science and engineering [13, 19, 37, 38]. This can be used to interpret dynamical systems irrespective of them being linear or non-linear [13]. However, the compromise is that the finite dimensional non-linear system may or may not require infinitely many

Date: June 06, 2023.

Key words and phrases. Deep Learning, Autoencoders, Data Driven Science, Reduced Order Modelling, Koopman Analysis.

Neranjaka Jayarathne is supported from the ONR.

Erik M. Boltt is supported by the ONR, ARO and AFSOR and the NIH-CRCN.

dimensions to be represented as a linear system. For most of the computations requirements a small error could be tolerated. Therefore the infinite dimensionality can be truncated at the cost of reduced accuracy. In their work [13] describes the foundations for this work. Furthermore, it explains why the low dimensional dataset could be used to do the same. This paper brings out a machine learning technique to reduce the dimensionality of the dataset produced by a dynamical system using deep autoencoders.

A *good dictionary* in this context refers to a set of eigenvectors for an efficient representations of the dynamical system. When representing arbitrary observable functions by a series of eigenvectors, there is freedom to define an efficient representation. Choosing the best from the rich and infinite eigenvectors develops a good dictionary of eigenvectors. The reader is referred to [5, 46, 48, 49] for *Koopman mood decomposition* as a global analysis of dynamical systems. This can be used to forecast as well as descriptive decompositions such as growing, fluctuating and decaying components.

The utility of the initial DMD and exact DMD methods as numerical techniques for computing Koopman eigenpairs persists, as evidenced by their continued use in research [13, 37, 53, 56]. Several variants of DMD exist, including sparse DMD [30], extended DMD (EDMD), and those that employ basis vectors to interpret data flow [35, 64]. In machine learning nomenclature, these basis vectors are commonly referred to as a *dictionary of features* [13]. Following this direction [41] describes an extended dynamic mode decomposition with optimal dictionary learning (EDMD-DL). DMD with control laws are introduced in [31, 37] which are emphasized on developing control laws.

In this paper we are developing a computationally efficient way of computing a good dictionary of Koopman eigen pairs. The technique of computing eigen pairs is based on [13]. Computational efficiency gain was induced by making a geometric transformation to the data manifold by means of deep learning techniques. In section 2 we present the mathematical and numerical foundations the Koopman eigen pairs are computed. In section 3 the machine learning technique was introduced. In section 4 examples are presented using the technique introduced. In section 5 the conclusions are derived with a direction for future developments.

2. MATHEMATICAL FOUNDATIONS

2.1. Koopman Analysis. First we review the underlying mathematics of Koopman analysis. Let,

$$(2.1) \quad \dot{X} = F(X), \quad F : M \rightarrow \mathbb{R}$$

be a dynamical system. The flow can be stated as a function for each $t \in \mathbb{R}$ such that $X(t) = \rho_t(X_0)$ where $X_0 = X(0) \in M$. This means that the trajectory starts at X_0 when $t = 0$. A *Koopman Operator* (KO) describes the evolution of observables along the flow [13, 19, 47]. This study is based on analyzing these observables. Let us call these observables as observation functions. With reference to [13], in this work we consider the observation function to be,

$$(2.2) \quad g : M \rightarrow \mathbb{C}$$

where,

$$(2.3) \quad g \in L^2(M) = \left\{ g : \int_M |g(s)|^2 ds < \infty \right\}$$

The scalar observation functions introduced here can be stacked to form vector observations. KO defines how the observation functions evolve over time along the orbits of the dynamical system.

Definition 2.1. Let ρ_t be a semiflow. That is, ρ_t is define for $t \geq 0$. Then the KO \mathbb{K}_t is defined for $L^2(M)$ such that,

$$(2.4) \quad \mathbb{K}_t[g](X) = g \circ \rho_t(X)$$

where, $\rho_t(X_0) = X_t$.

In lehman's terms, for each X we observe that value of an observable $g(x)$, not at x itself, but after a time t at $\rho_t(X)$. The KO is linear on $L^2(M)$. This may be at the cost of it being infinite dimensional. *eigenvectors* and *eigenvalues* are studied under the spectral analysis of the KO [19, 24, 47].

Definition 2.2. Suppose ϕ_λ is an eigenvector of \mathbb{K}_t and λ is the corresponding eigenvalue. Then the eigenpair should satisfy the equation,

$$(2.5) \quad \mathbb{K}_t[\phi_\lambda](X) = b^t \phi_\lambda(X) = e^{\lambda t} \phi_\lambda(X)$$

or

$$(2.6) \quad \mathbb{K}_t[\phi_\lambda](X) = e^{\lambda t} \phi_\lambda(X).$$

for each eigenvalue λ there are uncountable many eigenvectors. In general these are not linearly independent. It is interesting to explore how an observable function can be decomposed into eigenvectors of the KO .

Definition 2.3. Let $\overline{g(X)}$ be a vector of observable functions $g_k(X)$.

$$(2.7) \quad \overline{g(X)} = [g_1(X), \dots, g_D(X)] : M \rightarrow \mathbb{C}^D.$$

Suppose $\overline{g(X)}$ could be written as follows,

$$(2.8) \quad \overline{g(X)} = \sum_{j=1}^{\infty} \phi_{\lambda_j}(X) \mathbf{v}_j.$$

Then it follows that,

$$(2.9) \quad \overline{g(X_0)} = \sum_{j=1}^{\infty} \phi_{\lambda_j}(X_0) \mathbf{v}_j.$$

Apply KO to oth sides of the equation,

$$(2.10) \quad \mathbb{K} \overline{g(X_0)} = \mathbb{K} \sum_{j=1}^{\infty} \phi_{\lambda_j}(X_0) \mathbf{v}_j$$

$$(2.11) \quad g \circ \rho_t(X_0) = \sum_{j=1}^{\infty} \mathbb{K} [\phi_{\lambda_j}] (X_0) \mathbf{v}_j$$

where $X_t = X(t)$.

Since eigenvectors are not unique, the authors are interested in finding an efficient representation using eigenvectors.

Definition 2.4. In [13] a \mathbf{k} -efficient finite set of Koopman eigenpairs $\{\psi_{\lambda_i}(X)\}_{i=1}^k$ and $\{\phi_{\lambda_i}(X)\}_{i=1}^k$ be sets of \mathbf{k} unit eigenvectors.

Further let q be an observable function,

$$(2.12) \quad q : M \rightarrow \mathbb{C}.$$

If

$$(2.13) \quad \min_a \left\| \sum_{i=1}^k a_i \psi_{\lambda_i}(X) - q(X) \right\| \leq \min_b \left\| \sum_{i=1}^k b_i \phi_{\lambda_i}(X) - q(X) \right\|$$

then $\{\psi_{\lambda_i}(X)\}_{i=1}^k$ is a set of \mathbf{k} -efficient Koopman eigenvectors

2.2. Computational Technique of Determining Koopman Eigen Pairs.

Following definition of the eigenvector was rephrased from [13].

Theorem 2.5. *Let the Koopman eigenfunction PDE is defined for an ODE $\dot{X} = F(X)$, with a flow $X(r) = \rho_r(X_0) : M \times \mathbb{R} \rightarrow M$. Assume a co-dimension-one [1] initial data manifold $\Lambda \subset M$ that is non-recurrent for some time epoch, $r \in [t_1, t_2]$ that contains 0, and transverse to the flow, and let $\mathbb{U} = \cup_{t \in [t_1, t_2]} \rho_t(\Lambda)$ be the resulting non-recurrent closed domain. Furthermore, let $h : \Lambda \rightarrow \mathbb{C}$ be an initial data function then an Koopman eigen pair $(\lambda, \phi_\lambda(X))$ $\phi_\lambda : \mathbb{U} \rightarrow \mathbb{C}$ has the form,*

$$(2.14) \quad \phi_\lambda(X) = h \circ s^*(X) e^{\lambda r^*(X)}.$$

Now we present an computational explanation of the **Theorem 1.** of [13]. This is the mathematical infra structure of the work presented in this paper.

Suppose $\dot{X} = F(X)$ be an ODE satisfying the Koopman eigenvector PDE. Let the corresponding flow be given by $X(r) = \rho_r(X_0) : M \times \mathbb{R} \rightarrow M$. Further let $\Lambda \subset M$ be a co-dimension-one data manifold. We should pick a time interval where the data values are non-recurrent. Let us call this Λ a non-recurrent data manifold. Let us assume that the time span non-recurrent be $[t_1, t_2]$ and $0 \in [t_1, t_2]$.

If Λ is transverse to the flow, we can define \mathbb{U} as follows.

$$(2.15) \quad \mathbb{U} = \cup_{t \in [t_1, t_2]} \rho_t(\Lambda)$$

That is \mathbb{U} is the collection of all the trajectories starting from Λ . This includes reverse trajectories as well. Furthermore, let $h : \Lambda \rightarrow \mathbb{C}$ be an initial data function. Then an eigenpair $(\lambda, \phi_\lambda(X))$ satisfies the equation 2.14. where,

$$(2.16) \quad r^*(X) = \{t : \rho_{-t}(X) \cap \Lambda \neq \emptyset\}$$

and

$$(2.17) \quad s^* = s \circ \rho_{-r^*(X)}(X)$$

Where s is the parametrization of Λ . That is, s is the data function available on Λ .

The exercise of [13] was to introduce this formulation and introduce the algorithm to numerically compute h and optimal λ for a given stream of data.

Following is a summary of the numerical algorithm described in [13].

Suppose $q \in L^2(\mathbb{U})$ be an arbitrary data function. $q : \mathbb{U} \rightarrow \mathbb{C}$. Let,

$$(2.18) \quad \psi = \operatorname{argmin}_{\lambda, h} \|\phi_{\lambda, h} - q\|_{L^2(\mathbb{U})}^2$$

be the eigenvector that closely estimates q . $\psi : \mathbb{U} \rightarrow \mathbb{C}$. It is worth noting that the optimization is over both λ and h . Further more,

$$(2.19) \quad \operatorname{argmax}_{\lambda, h} (q, \phi_{\lambda, h}) = \operatorname{argmin}_{\lambda, h} \|\phi_{\lambda, h} - q\|_{L^2(\mathbb{U})}^2$$

where,

$$(2.20) \quad \|f\|_{L^2(\mathbb{U})} = \int_{\mathbb{U}} f(X) dX$$

and

$$(2.21) \quad (f, g) = \int_{\mathbb{U}} f(X) g(X) dX$$

for any $f, g \in L^2(\mathbb{U})$.

Let us explain an example scenario for a 2-dimensional dynamical system. The algorithm can be generalized to larger dimensions limited only by the computational resources. Then Λ becomes 1-dimensional since it should be co-dimension 1. let $s_0 < s_1 < \dots < s_n$ be a uniform partition of Λ . The data function $h : \Lambda \rightarrow \mathbb{C}$ could be indexed accordingly as

$$(2.22) \quad h_i := h(s_i)$$

We will consider a uniform grid of time as well. $r_0 = 0 < r_1 < \dots < r_m$. That is $m+1$ number of equal time steps. Then the grid points can be identified as follows $s_{i,j} = \rho_{r_j} \circ x(s_i)$, $0 \leq i \leq m$, $0 \leq j \leq m$.

Then in terms of the grid, the optimization problem in equation 2.18 for the function $\psi(x)$ represented on the grid $\psi \circ x(s_{i,j})$ is approximated by solving the finite rank least squares problem.

$$(2.23) \quad \tilde{\psi} = \operatorname{argmin}_h \|\phi_{\lambda, h} \circ x(s_{i,j}) - q \circ x(s_{i,j})\|_F^2 = \operatorname{argmin}_{h_i} \sum_{j=1}^m \sum_{i=1}^n |e^{\lambda r_j} h_i - q_{i,j}|^2$$

On this grid both functions q and $\tilde{\psi}_{\lambda, h}$ can be sampled at $\rho_{r_j} \circ x(s_i)$.

$q_{i,j} = q(s_{i,j})$ for $0 \leq i \leq n$, $0 \leq m$. In [13], for distance the Frobenius norm [2] is used.

We can rewrite the optimal initial data as an $n \times 1$ vector $h^0(\lambda) \in \mathbb{C}^n$. The problem restatement is as follows.

Let us define the $m \times 1$ vector $E(\lambda)$ as $E(\lambda) = [e^{\lambda r_0} \ e^{\lambda r_2} \ \dots \ e^{\lambda r_m}] \in \mathbb{C}^m$.

Then $A(\lambda) = E(\lambda) \otimes I_n$ where \otimes is the Kronecker product. Furthermore, let b be the vector received by reshaping the matrix $q \in \mathbb{C}^{n \times m}$ into a vector of shape $mn \times 1$. That is $b = \operatorname{reshape}(q, mn, 1)$.

Then $h^0(\lambda)$ is computed by solving the least squares problem,

$$(2.24) \quad h^0(\lambda) = \operatorname{argmin}_h \|A(\lambda)h - b\|_2$$

It is noticed that $q = q(s_{i,j})$ is a grid of values. It follows that,

$$(2.25) \quad p^0(\lambda) = A(\lambda)h^0(\lambda)$$

Then $\tilde{\psi}_1^0 = \operatorname{reshape}(p^0(\lambda), n, m)$.

That is, in order to produce the optimal eigenvector, $p^0(\lambda)$ is being reshaped.

$\tilde{\psi}_1^0$ is the eigenvector computed by carrying out the computation once. This can be successively done to reduce the residuals.

Therefore we can call the residue at the k th iteration R_k .

Then,

$$(2.26) \quad R_k = b - \sum_{i=1}^k p_i^0$$

Then the successive eigen pairs can be computed by using,

$$(2.27) \quad (\lambda_{k+1}^0, \lambda_{k+1}^0) = \operatorname{argmin}_{\lambda, h} \|A(\lambda)h - R_k\|_2$$

$$(2.28) \quad \tilde{\psi}_{k+1}^0 = \operatorname{reshape}(p_k^0, n, m)$$

3. MANIFOLD LEARNING

In [1] and [23] a manifold is described as a collection of charts which is called atlas. Each chart maps a subset of the manifold to the *Euclidean Space* with an invertible map. These subsets could have intersections which are not empty. The invertible maps should be consistent in the non empty intersections. Further more, a manifold is a topological space which is *Locally Euclidean* [1].

3.1. Manifold Hypothesis. The manifold hypothesis is the assumption that higher dimensional data lie on lower dimensional manifolds embedded within the higher dimensional space [22, 50]. This is due to the belief that high dimensional data could be generated from a low dimensional dynamical system. Specifically in the context of a dynamical system, orbit data may be attracted to a stable invariant manifold, which occurs in certain systems where dissipation leads to the potential of a reduced order model. A collection of techniques developed to identify such a low dimensional manifold using the available high dimensional data is called manifold learning. For a comprehensive study of the manifold hypothesis and its mathematical consequences the reader is referred to [22].

3.2. Manifold Learning. Among the handful of manifold learning techniques a few techniques such as isometric feature mapping *ISOMAP*, Locally Linear Embeddings (*LLE*), Laplacian Eigenmaps, Diffusion Maps, Nonlinear Principal Component Analysis stands out from the rest. While introducing manifold learning, [29] introduces it as an algorithmic technique for dimensionality reduction. In there paper [61] introduces a geometric framework for nonlinear dimensionality reduction. The authors claim that their technique efficiently computes the global optimal and it is guaranteed to converge asymptotically to the true structure. For a comprehensive study of *LLE* the reader is referred to [52]. For treatment of *ISOMAP* algorithms and *Laplacian Eigen Maps* the interested reader is referred to [8] and [9] respectively. However this investigation is more interested about manifold learning using deep learning techniques. Following is a concise empirical study of deep learning based manifold learning in various engineering applications. For a more descriptive treatment on topological point of view of manifold learning refer to [23].

3.3. Mathematical Foundations of Manifold Learning. Dimensional reduction of the data is the main application of manifold learning. The data which is to be dimensionally reduced is assumed to be generated from a lower dimensional submanifold [45]. A d -dimensional manifold M has the property that for all $x \in M$ there is a neighborhood $X_x \subset M$ of x such that X_x is homeomorphic to an open set $\Theta_x \subset \mathbb{R}^d$ where \mathbb{R}^d is the d -dimensional Euclidean space [16]. Then Θ_x can be called a local coordinate of X_x [16].

Since $M = \bigcup_{x \in M} X_x$ where $\{X_x | x \in M\}$ is an *open covering* of M . We can find an homeomorphism $\phi_x : X_x \rightarrow \Theta_x$ for all $x \in M$. Then for all $x \in M$, we have $\phi_x(X_x) = \Theta_x$. Therefore $\{\Theta_x | x \in M\}$ can be represented as $\{(X_x, \Theta_x) | x \in M\}$. The set of homeomorphisms $\{\phi_x\}_{x \in M}$ need not be unique [16]. This leads to the observation that learnt manifolds need not be unique. Suppose $X = \{X_1, X_2, \dots, X_N\} \subset M \subset \mathbb{R}^{d'}$ be the set of observable data vectors. Let $Y = \{Y_1, Y_2, \dots, Y_N\} \subset \mathbb{R}^d$ be the reduced dimensional vectors where $d' > d$. It can then be concluded that the observable data was generated by a d -dimensional dynamical system. Finding the homeomorphism $\phi : X \rightarrow Y$ such that $\phi(X_i) = Y_i$ for $1 \leq i \leq N$ is the process of manifold learning.

Even though the previously surveyed techniques can be used for manifold learning, this investigation is interested about deep learning techniques. The deep learning techniques are favourable in real time computing and the learnt deep neural network can be used to uncover the intrinsic local coordinates. This ability comes as a consequence of the results of this investigation.

Following is a concise survey of applications of deep manifold learning. While introducing the phrase *Deep Manifold Learning (DML)* for deep learning for hidden less dimensional manifolds [20] represents a framework of DML for action recognition using convolutional Neural Networks. In their paper on image set classification [63] introduces a technique for *Riemannian* manifold deep learning. This paper also provides a summary of previous efforts on Riemannian manifold learning.

3.4. Autoencoders. Autoencoders have become a standout machine learning method to find a reduced order model in an invariant manifold within an artificial neural network framework, including in dynamical systems with stable reduced order models [40, 7]. Figure 1 depicts a basic neural network topology of a deep autoencoder.

Autoencoders (AE) were first proposed and formulated by the PhD thesis of Y. LeCun [39]. These are traditionally used for dimensionality reduction [65]. Based on the formulation of [26] the mathematical foundation of an AE can be viewed as a recursive formula 3.1. The mathematical foundation of the neural networks can be found in [12].

$$(3.1) \quad x^{(l)} = g \left(b^{(l-1)} + W^{(l-1)} x^{(l-1)} \right)$$

Let $K^{(l)}$ denote the number of neurons in each layer where, $l = 1, 2, 3, \dots, L$. Let the output of neuron k in layer l be $x_k^{(l)}$, and the vector of all outputs for this layer as $x^{(l)} = \left(x_1^{(l)}, x_2^{(l)}, x_3^{(l)}, \dots, x_{K^{(l)}}^{(l)} \right)'$. In each node, a nonlinear activation function $g(\cdot)$ is applied further to the linear operation. In the recursive equation 3.1, $W^{(l-1)}$ is a $K^{(l)} \times K^{(l-1)}$ matrix of weight parameters, and $b^{(l-1)}$ is a $K^{(l)} \times 1$ vector of

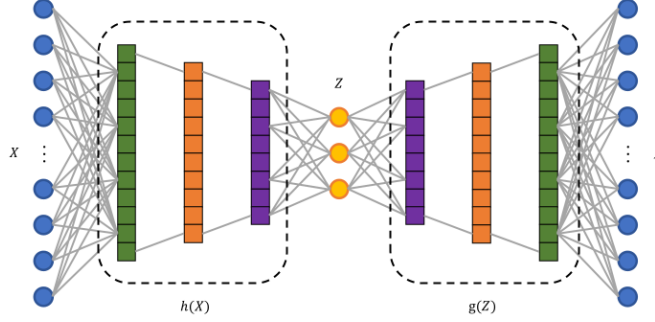


FIGURE 1. Graphical depiction of a simplified deep autoencoder

bias parameters [26]. For this work, "sigmoid" and "ReLU" [33] were proven to be acceptable activation functions. We decided to do our experiments with *sigmoid* consistently.

Autoencoders, in general, takes the form $Z = h(X)$ and $\hat{X} = g(Z)$, where \hat{X} is the output of the neural network. Vector value Z is known as the latent vector, which is the encoded/transformed form of X . Transformation g suppose to invert the transformation h . Therefore, ideally, $g = h^{-1}$. The loss function of the neural network is a function of $\|\hat{X} - X\|$. We used the mean squared error as the loss function,

$$(3.2) \quad \mathbb{L} = \frac{1}{N} \sum_{i=1}^N \|\hat{X} - X\|^2$$

Subsequently \mathbb{L} is minimized using the gradient descent over a multitude of iterations.

3.5. Autoencoders for Reduced Order Modeling. Full order models require increased utilization of resources. The main goal of a reduced representation is to capture the essential physical features of a system and project them onto a lower-dimensional space or manifold in a way that preserves as much information as possible, while still allowing for meaningful comparisons to be made with a full-order model (FOM). This approach is therefore called reduced order modeling (ROM) [51]. There have been many attempts in developing ROMs for dynamical systems [6, 44, 34]. Compiling a ROM for a complex dynamical system could be challenging task. Compiling a ROM for a complex dynamical system can be an exceedingly arduous task due to the inherent complexity of the system. The projection-based ROM is one of the earliest and most widely used techniques for reduced order modeling. This method involves transforming the original space into a lower-dimensional space using the governing PDEs (Partial Differential Equations) of the physical system [55].

Proper Orthogonal Decomposition (POD) is a widely used projection-based ROM technique, particularly in the field of computational fluid dynamics. It involves decomposing the original data into a set of orthogonal modes that capture the dominant dynamics of the system. For those interested in delving deeper into the topic of POD, we recommend referring to the following seminal works: [4, 11, 27]. Principal Component Analysis (PCA) [28] is a comparable method to POD which gathered momentum due to the availability of the computing resources. Empirical orthogonal functions [43] Karhunen-Loeve expansion [42] are also similar techniques for ROM. According to [59] these ROM techniques utilize the eigen-decomposition of the snapshot matrix using Singular Value Decomposition (SVD).

Dynamic Mode Decomposition (DMD) is a ROM technique which is popular in modeling physics based systems using there spatio-temporal coherent structures [53]. DMD is being used for a wide range of applications[18]. Image-processing [57], Neuroscience [17], and Robotics [10] are to name a few. Koopman operator theory (KOT) itself has direct connections to DMD. KOT was early used for characterization of the dynamics of the Hamiltonian functions [36]. An Extended version of DMD (EDMD) was used in [41] to decompose the KOT for the analysis of a non-linear dynamical system. A matching dynamical system is formed using the Koopman operator by decomposing the operator using EDMD in [14].

4. EXAMPLES

Now we provide couple of worked examples of the developed theory.

4.1. Example 1: Van der Pol Oscillator. We use the *Van der Pol* (*VdP*) oscillator as the first example for simulation. *VdP* is an oscillator with non linear damping [32]. First step of the process is to simulate trajectories of the *VdP*. In order to simulate geometric transformations using deep autoencoders, we considered a complete cycle of each trajectory. These trajectories are similar to what is depicted in figure 3. The original trajectories lie on 2 dimensional plane. Then we projected these trajectories to a 3 dimensional space using the mapping,

$$(4.1) \quad \begin{bmatrix} \bar{x}_1 \\ \bar{x}_2 \\ \bar{x}_3 \end{bmatrix} = \begin{bmatrix} x_1 \\ x_2 \\ x_1^2 + x_2^2 \end{bmatrix}.$$

This transforms $2d$ trajectories in to trajectories in $3d$. These projected trajectories are depicted in figure 2. At this state the dynamical system is treated as a 3 dimensional system. The next step would be to reduce the order of the model to 2. We did it using a deep-autoencoder(*DAE*). Following is a brief description of the *DAE* we tuned for this particular system. For implementing the deep neural network, we used *Keras* which is based on *Tensorflow*. Both of these were programmed using *python* programing language. The *DAE* had the latent vector size of 2, consistent with our goal. We received optimal results when the first and second hidden layers had the sizes of 100 nodes each. These two hidden layers are the encoder. The decoder, which is the neural network after the latent vector, has the same architecture as the encoder. Optimal results were received when *Sigmoid* was used as the activation function. Comparably similar results were achieved when Rectified Linear Unit(*Relu*) was used as the activation function. *tanh* and *softmax* functions did not comparably similar results. These two functions were rejected after visually inspecting the resulting reduced order trajectories. All the layers in

the neural network were dense. As a normalized practice, the networks were trained for 2000 epochs throughout the study. Before feeding into the neural network for training, each stream of data has to be scaled from 0 to 1. The scaled 2 dimensional trajectories are depicted in figure 3. There are many trajectories each with a different initial point. The nature of the *VdP* is that they converge to a stable limit cycle. The range of initial points are depicted by the anomaly at around the points $(0.9, 0.5)$ and $(1, 0.5)$ in figure 3. All the trajectories, initiated from the range of different initial points eventually converges to the stable limit cycle and stay on it. Therefore, it is sufficient to simulate one initial period. The transformed trajectory is depicted in figure 4. There is no guarantee that the transformed trajectory will always be this. Even with the original trajectories being the same the autoencoder might converge to a different local minimum of the error producing a different transformation. Finding a geometric transformation using an *DAE* is a trial and error process. The number of hidden layers, number of nodes on each layer, number of epochs to train, the activation function may vary with the application at hand. Therefore it is, to be found and optimized over several iterations during the process of simulation.

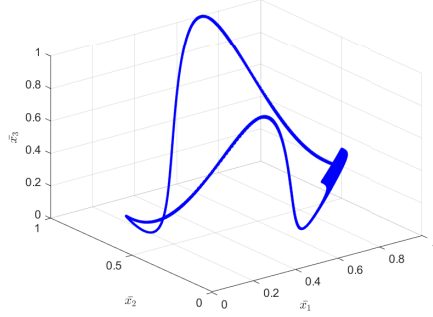


FIGURE 2. Trajectories from the Van der Pol Oscillator projected on to the 3 dimensions and scaled

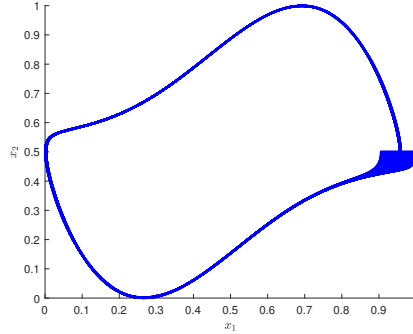


FIGURE 3. Scaled trajectories from the Van der Pol Oscillator

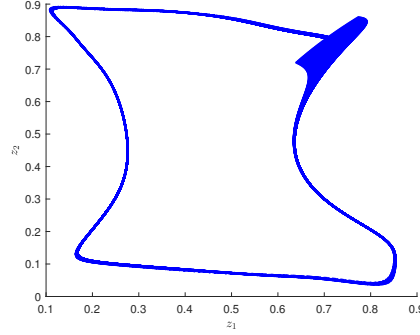


FIGURE 4. Transformed trajectories from the Van der Pol Oscillator

4.2. Reduced Order Modeling for Koopman Eigen Pair Computation.

Now we move into the analysis of the geometric transformation of the trajectory we used for *Koopman* eigen pair computation. For the *Koopman* analysis we do not need a full cycle of a trajectory. Therefore the trajectories are restricted to a shorter time period. The scaled trajectory is depicted in figure 5. Again this is projected to the 3 dimensional space using the same transformation as in the complete trajectory case. The same neural network architecture as for the previous case was used to autoencode the set of shorter trajectories. The reduced order model (*ROM*) trajectories are depicted in figure 7. A closer comparison between figures 4 and 7 will hint the interested reader that the two transformations are not equal to each other. For the *DAE*, the same architecture and hyper-parameters were used as the full trajectory *DAE*. This guarantees that accuracy is going to converge to a stable value. The next step is to use the *ROM* to compute the *Koopman* eigenvectors and eigenvalues.

4.3. Computing Koopman Eigenvectors with the *ROM*. This phase is to find *Koopman* eigenvectors as given by the equation 2.14. As given by the equation 2.17, s^* is derived as a consequence of the flow of the dynamical system. This leads to the fact that, we only need to determine the optimal eigenvalue λ and the corresponding h of the equation 2.14. To be consistent with the investigation of [13] we chose the observation function to be $q = 3e^{-\frac{x_1^2 + x_2^2}{10}}$. When x_i s are replaced by z_i s we get, $q = 3e^{-\frac{z_1^2 + z_2^2}{10}}$. In this case, instead of using x_1 and x_2 we use z_1 and z_2 , the transformed coordinates. We computed the first 10 modes or the first eigenvectors and their corresponding eigenvalues. For each mode the corresponding eigenvalue is the value of λ which minimizes the error which is depicted in figure 8. The $h(s)$ vectors for the first 10 modes are depicted in 9. The absolute error between the sum of eigenvectors and the observation function decreases with the mode. This is depicted in figure 10.

4.3.1. eigenpairs with a Different Observation Function. Now we change the observation function to $q = z_1^2 + z_2^2$. The variation of the error with λ and the function $h(s)$ for the first 10 modes are plotted in sub-figures, 11a and 11b respectively. The corresponding minimum error vs mode graph is presented in figure 12

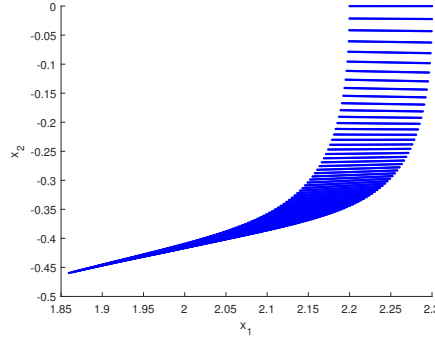


FIGURE 5. Trajectories from the Van der Pol Oscillator

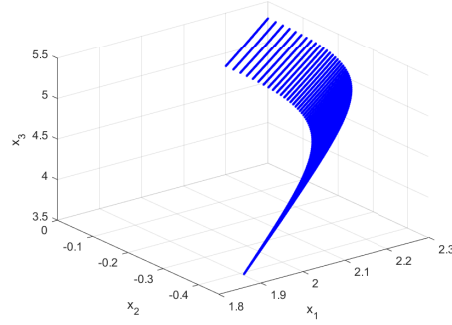


FIGURE 6. Trajectories from the Van der Pol Oscillator projected to 3 dimensional space

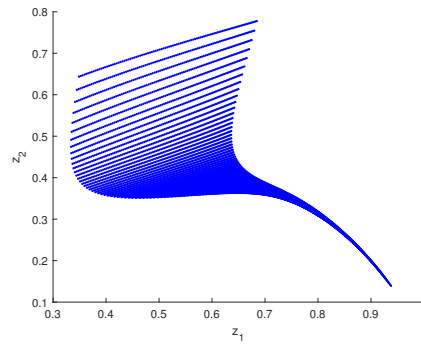
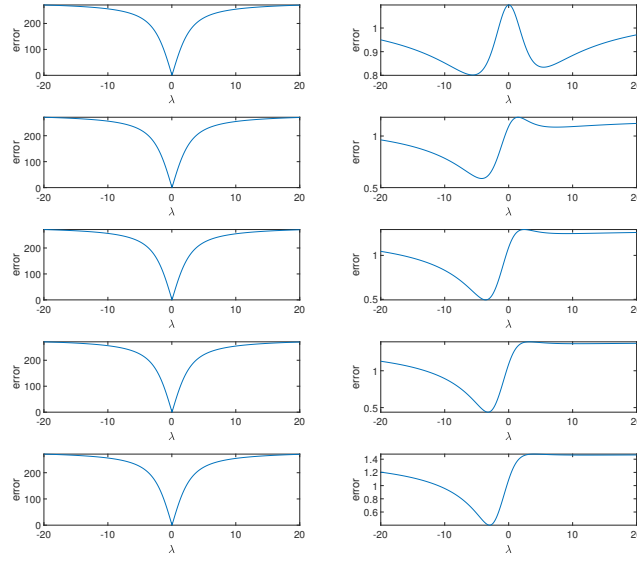
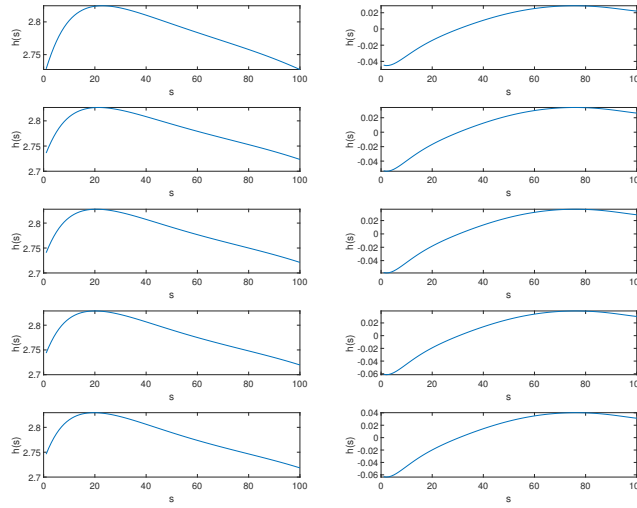


FIGURE 7. Trajectories in the transformed geometry

4.4. Example 2: Reaction Diffusion. Now we apply our algorithm to a 1 dimensional reaction diffusion equation which appears in [62].


 FIGURE 8. Error vs λ variation through the first 10 modes

 FIGURE 9. $h(s)$ of the first 10 modes

$$\begin{aligned}
 (4.2) \quad \frac{\partial u_1}{\partial t} &= D \frac{\partial^2 u_1}{\partial x^2} + \frac{1}{\epsilon} (u_2 - f(u_1)) \\
 \frac{\partial u_2}{\partial t} &= D \frac{\partial^2 u_2}{\partial x^2} - u_1 + \alpha
 \end{aligned}$$

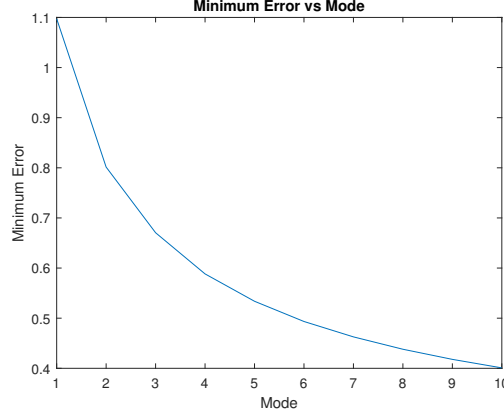
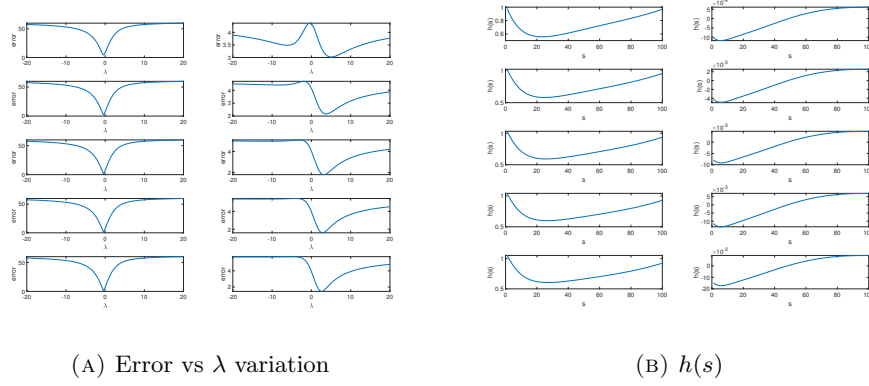


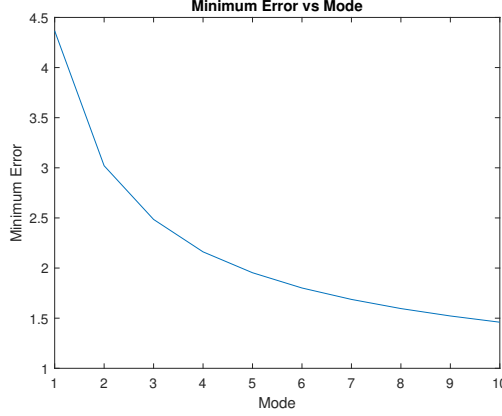
FIGURE 10. Minimum Error vs. Mode

FIGURE 11. VdP trajectories with $q = z_1^2 + z_2^2$

In the system 4.2, $x \in [0, 1]$ and it is subject to *Dirichlet* conditions,

$$(4.3) \quad \begin{aligned} u_1(x=0, t=0) &= u_1(x=1, t=0) \\ u_2(x=0, t=0) &= u_2(x=1, t=0). \end{aligned}$$

We chose to fix $\epsilon = 0.01$ and $\alpha = 0.01$ for our experiments. The simulation we have presented, we used $D = 0.0322$. The surface plots for u_1 and u_2 for these parameters are presented in the figure 13 where $x \in [0, 1]$ and $0 \leq t \leq 60$. It is noted that this reaction-diffusion system produces chaotic [25] behavior depending on the values of ϵ and D . The trajectories of u_1 and u_2 at $x = 1/2$ are graphed in figure 14. Even though mathematically, there are unaccountably many trajectories between $x = 0$ and $x = 1$, computationally this number is countably finite. We used x to be *linspace*(0,1,100). This leads to the resulting simulation having 100 trajectories. When there are 100 trajectories each for u_1 and u_2 there are 200 trajectories. Each trajectory from these becomes an input to the DAE. In order the machine learn an reduced order model, the deep neural network had to have at least 4000 nodes in


 FIGURE 12. Minimum Error vs. Mode for $q = z_1^2 + z_2^2$

the first hidden layer. The network architecture with (4000, 4000) did not converge beyond 25% accuracy. Increasing the number of nodes to (10000, 1000) did not improve the accuracy significantly. The available computing cloud resources were not sufficient to increase the number of nodes further. Therefore we had to look for other means of producing the reduced order model.

The solution we found was to pre-process the data using other means. In particular, we used another embedding technique using time delayed snapshots of the trajectories.

4.5. Takens's Time Delay Embedding. Takens's theorem provides conditions where we can reproduce the dynamical system using sequential data from a single trajectory rather than processing all the trajectories in parallel. Since all the trajectories from the reaction-diffusion cannot be processed together in parallel with available computing resources, Takens's theorem can be used to reconstruct the dynamical system using time delay embedding with one trajectory at a time.

Takens's time delay embedding was introduced in the paper [60]. This provides conditions under which a smooth attractor can be reconstructed from the observations made with an observable function. Suppose we have a d -dimensional dynamical system given by a state vector x_t which is continuous. Further, assume that we have one observable function $y(t)$ which is coupled to all components of x_t . Then a k dimensional vector of observations can be created by considering k time lagged observations with period τ of $y(t)$, that is $[\dots, y_{t-2\tau}, y_{t-\tau}, y_t, y_{t+\tau}, y_{t+2\tau}, \dots]$ so on and so forth. As $k \rightarrow \infty$ the system becomes deterministic and predictable. The *Takens's* theorem states that the dynamics of the lagged vector becomes deterministic at a finite dimension. The finite dimension is given by $k < 2d + 1$.

Let us present the *Takens's* embedding theorem more formally.

Theorem 4.1 (Takens's Embedding Theorem). *Let $\dot{X} = f(X)$ be a dynamical system defined on the manifold M . $f : M \mapsto M$ and f is smooth. Suppose that the dynamics f has the strange attractor [54] \mathbb{A} with Minkowski-Bouligand dimension [21] $d_{\mathbb{A}}$. Using the Whitney's embedding theorem [3], [58], \mathbb{A} can be embedded in k -dimensional Euclidean space with $k > 2d_{\mathbb{A}}$. That is there is a diffeomorphism ϕ that maps \mathbb{A} into \mathbb{R}^k such that the derivative of ϕ has full rank.*

Building on theorem 4.1, it is possible to construct a vector using only a single trajectory from the flow of trajectories of 4.2. In the work presented in this paper each of the trajectories u_1 and u_2 are time embedded into a vector of size 5. It is further explained by using the trajectory at $x = 1/2$. The values of the trajectory at $x = 1/2$ are isolated for both u_1 and u_2 . Since the values are discrete, τ is taken to be the time steps available. Let the time stamp we are considering to be $t = t_0$. Then the scalar $u_1(x = 1/2, t = t_0)$ is composed to be a vector given by,

$$\begin{bmatrix} u_1(x = 1/2, t_0 - 2) \\ u_1(x = 1/2, t_0 - 1) \\ u_1(x = 1/2, t_0) \\ u_1(x = 1/2, t_0 + 1) \\ u_1(x = 1/2, t_0 + 2) \end{bmatrix}.$$

$[u_1(x = 1/2, t_0 - 2), u_1(x = 1/2, t_0 - 1), u_1(x = 1/2, t_0), u_1(x = 1/2, t_0 + 1), u_1(x = 1/2, t_0 + 2)]^T$.
When both u_1 and u_2 are considered, it becomes the following vector.

$$\begin{bmatrix} u_1(x = 1/2, t_0 - 2) \\ u_1(x = 1/2, t_0 - 1) \\ u_1(x = 1/2, t_0) \\ u_1(x = 1/2, t_0 + 1) \\ u_1(x = 1/2, t_0 + 2) \\ u_2(x = 1/2, t_0 - 2) \\ u_2(x = 1/2, t_0 - 1) \\ u_2(x = 1/2, t_0) \\ u_2(x = 1/2, t_0 + 1) \\ u_2(x = 1/2, t_0 + 2) \end{bmatrix}$$

Then the trajectories for different x values are fed to the neural network serially.

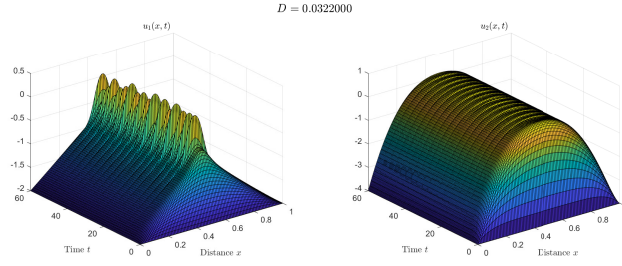
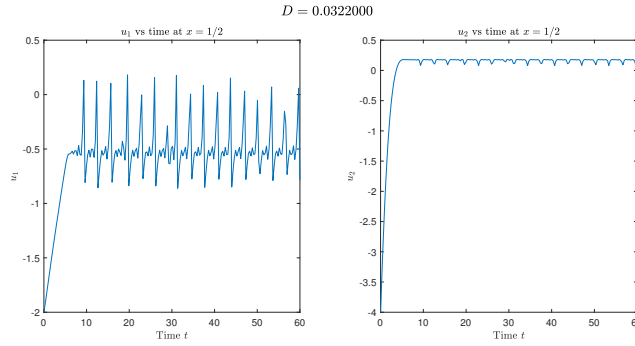
The first hidden layer had 3200 nodes while the second hidden layer had 100 nodes with a latent vector size of 6 the network produced an accuracy $> 70\%$. Using this reduced order model the *Koopman* eigenvectors were computed.

For the simulation of the eigen pair computations, $q = 3e^{-\frac{z_1^2 + z_2^2 + z_3^2 + z_4^2 + z_5^2 + z_6^2}{10}}$ was taken as the observations function. Similar to the previous experiment we have produced the graphs corresponding to the first 10 modes.

Figure 15 displays graphs that illustrate how the error changes with the eigenvalue of the initial 10 modes. The binary nature of the graphs are observed again. While the graphs of the odd modes exhibit a similar shape, the graphs of the even modes display a shape that is different but yet similar to each other. Figure 16 depicts the graphs of the computed $h(s)$ functions of the corresponding modes. It is visible that there is a "saw-tooth" nature to all the graphs even though there are two distinctive types of graphs. Figure 17 depicts the error variation with mode. The absolute error is initially around 8.9 but decreases to slightly below 8.4, where it then remains constant.

5. CONCLUSIONS AND FURTHER WORK

In this paper we were trying to bring out deep autoencoding as a technique for uncovering simple geometries of complex dynamical systems. Autoencoder works as a geometric transformation. The transformed stream of data is then used to compute a dictionary of Koopman eigen pairs. The technique used to compute


 FIGURE 13. Surface plots of u_1 and u_2 of Reaction-Diffusion PDE

 FIGURE 14. u_1 and u_2 at $x = 1/2$ of Reaction-Diffusion PDE

Koopman eigen pairs is different from the conventional technique and is introduced in the paper [13]. In that paper the eigen pairs are determined using the data streams as it is presented. In this paper, we improve on that and compute the eigen pairs using the transformed geometry.

The transformation minimizes the vector size of the input data by compressing the data driven dynamical system into a low dimensional manifold. This reduces the required computational resources to compute the eigen pairs. The transformed data stream is then a reduced order model of the full order dynamical system.

When this *ROM* is formed using an autoencoder there is no technique to make this model according to our need. This is because the autoencoder is an unsupervised learning technique. To overcome this, a non-trivial loss function can be introduced. This loss function could partly depend on the latent variables and partly on the output of the neural network. Even though this is still unsupervised learning, the *ROM* can be governed using a non trivial loss function. This will, in turn, lead to less error in Koopman eigen pair calculations.

REFERENCES

- [1] Ralph Abraham and Jerrold E Marsden, *Foundations of mechanics*, no. 364, American Mathematical Soc., 2008.
- [2] Azmy S Ackleh, Edward James Allen, R Baker Kearfott, and Padmanabhan Seshaiyer, *Classical and modern numerical analysis: theory, methods and practice*, Crc Press, 2009.
- [3] Masahisa Adachi, *Embeddings and immersions*, American Mathematical Soc., 2012.

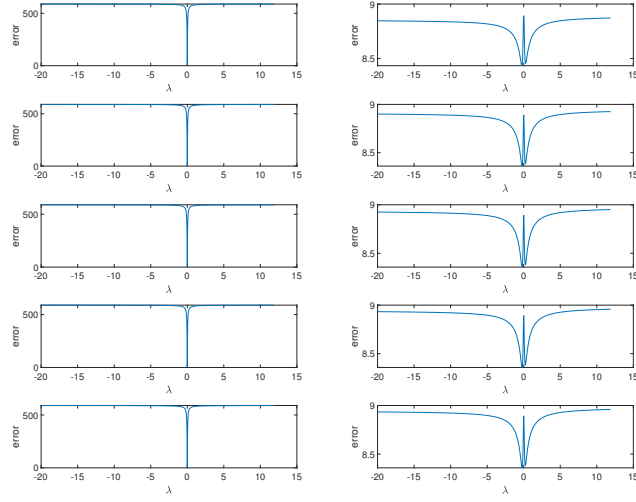


FIGURE 15. Error vs λ variation through the first 10 modes Reaction-Diffusion PDE

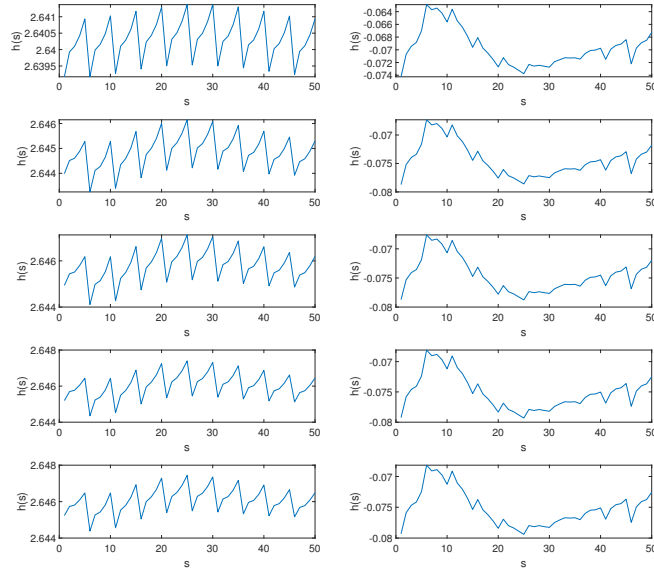


FIGURE 16. $h(s)$ of the first 10 modes Reaction-Diffusion PDE

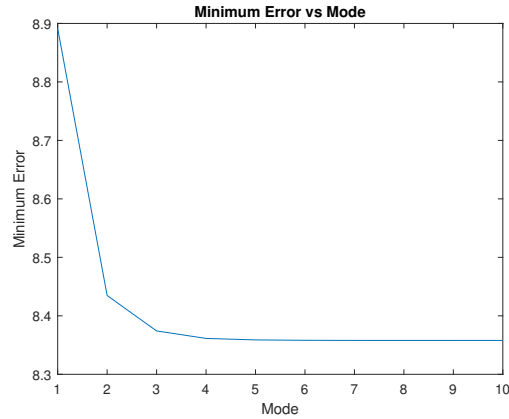


FIGURE 17. Minimum Error vs. Mode Reaction-Diffusion PDE

- [4] Nadine Aubry, Philip Holmes, John L Lumley, and Emily Stone, *The dynamics of coherent structures in the wall region of a turbulent boundary layer*, Journal of fluid Mechanics **192** (1988), 115–173.
- [5] Allan M Avila and I Mezić, *Data-driven analysis and forecasting of highway traffic dynamics*, Nature communications **11** (2020), no. 1, 1–16.
- [6] Zhaojun Bai, *Krylov subspace techniques for reduced-order modeling of large-scale dynamical systems*, Applied numerical mathematics **43** (2002), no. 1-2, 9–44.
- [7] Joseph Bakarji, Kathleen Champion, J Nathan Kutz, and Steven L Brunton, *Discovering governing equations from partial measurements with deep delay autoencoders*, arXiv preprint arXiv:2201.05136 (2022).
- [8] Mukund Balasubramanian and Eric L Schwartz, *The isomap algorithm and topological stability*, Science **295** (2002), no. 5552, 7–7.
- [9] Mikhail Belkin and Partha Niyogi, *Laplacian eigenmaps and spectral techniques for embedding and clustering*, Advances in neural information processing systems **14** (2001).
- [10] Erik Berger, Mark Sastuba, David Vogt, Bernhard Jung, and Heni Ben Amor, *Dynamic mode decomposition for perturbation estimation in human robot interaction*, The 23rd IEEE International Symposium on Robot and Human Interactive Communication, IEEE, 2014, pp. 593–600.
- [11] Gal Berkooz, Philip Holmes, and John L Lumley, *The proper orthogonal decomposition in the analysis of turbulent flows*, Annual review of fluid mechanics **25** (1993), no. 1, 539–575.
- [12] Christopher M Bishop and Nasser M Nasrabadi, *Pattern recognition and machine learning*, vol. 4, Springer, 2006.
- [13] Erik M Bollt, *Geometric considerations of a good dictionary for koopman analysis of dynamical systems: Cardinality, “primary eigenfunction,” and efficient representation*, Communications in Nonlinear Science and Numerical Simulation **100** (2021), 105833.
- [14] Erik M Bollt, Qianxiao Li, Felix Dietrich, and Ioannis Kevrekidis, *On matching, and even rectifying, dynamical systems through koopman operator eigenfunctions*, SIAM Journal on Applied Dynamical Systems **17** (2018), no. 2, 1925–1960.
- [15] Erik M Bollt and Naratip Santitissadeekorn, *Applied and computational measurable dynamics*, SIAM, 2013.
- [16] William M Boothby and William Munger Boothby, *An introduction to differentiable manifolds and riemannian geometry, revised*, vol. 120, Gulf Professional Publishing, 2003.
- [17] Bingni W Brunton, Lise A Johnson, Jeffrey G Ojemann, and J Nathan Kutz, *Extracting spatial-temporal coherent patterns in large-scale neural recordings using dynamic mode decomposition*, Journal of neuroscience methods **258** (2016), 1–15.
- [18] Steven L Brunton and J Nathan Kutz, *Data-driven science and engineering: Machine learning, dynamical systems, and control*, Cambridge University Press, 2022.

- [19] Marko Budišić, Ryan Mohr, and Igor Mezić, *Applied koopmanism*, Chaos: An Interdisciplinary Journal of Nonlinear Science **22** (2012), no. 4, 047510.
- [20] Xin Chen, Jian Weng, Wei Lu, Jiaming Xu, and Jiasi Weng, *Deep manifold learning combined with convolutional neural networks for action recognition*, IEEE transactions on neural networks and learning systems **29** (2017), no. 9, 3938–3952.
- [21] Kenneth Falconer, *Fractal geometry: mathematical foundations and applications*, John Wiley & Sons, 2004.
- [22] Charles Fefferman, Sanjoy Mitter, and Hariharan Narayanan, *Testing the manifold hypothesis*, Journal of the American Mathematical Society **29** (2016), no. 4, 983–1049.
- [23] Daniel Floryan and Michael D Graham, *Charts and atlases for nonlinear data-driven models of dynamics on manifolds*, arXiv preprint arXiv:2108.05928 (2021).
- [24] Pierre Gaspard, *Chaos, scattering and statistical mechanics*, Chaos (2005).
- [25] Herbert Goldstein, Charles Poole, and John Safko, *Classical mechanics*, 2002.
- [26] Shihao Gu, Bryan Kelly, and Dacheng Xiu, *Autoencoder asset pricing models*, Journal of Econometrics **222** (2021), no. 1, 429–450.
- [27] Philip Holmes, John L Lumley, Gahl Berkooz, and Clarence W Rowley, *Turbulence, coherent structures, dynamical systems and symmetry*, Cambridge university press, 2012.
- [28] Harold Hotelling, *Analysis of a complex of statistical variables into principal components.*, Journal of educational psychology **24** (1933), no. 6, 417.
- [29] Alan Julian Izenman, *Introduction to manifold learning*, Wiley Interdisciplinary Reviews: Computational Statistics **4** (2012), no. 5, 439–446.
- [30] Mihailo R Jovanovic, Peter J Schmid, and JW Nichols, *Low-rank and sparse dynamic mode decomposition*, Center for Turbulence Research Annual Research Briefs **2012** (2012), 139–152.
- [31] Eurika Kaiser, J Nathan Kutz, and Steven L Brunton, *Data-driven approximations of dynamical systems operators for control*, The Koopman Operator in Systems and Control: Concepts, Methodologies, and Applications (2020), 197–234.
- [32] Takashi Kanamaru, *Van der pol oscillator*, Scholarpedia **2** (2007), no. 1, 2202.
- [33] Bekir Karlik and A Vehbi Olgac, *Performance analysis of various activation functions in generalized mlp architectures of neural networks*, International Journal of Artificial Intelligence and Expert Systems **1** (2011), no. 4, 111–122.
- [34] Nikolaos Kazantzis, Costas Kravaris, and Lemonia Syrou, *A new model reduction method for nonlinear dynamical systems*, Nonlinear Dynamics **59** (2010), 183–194.
- [35] I Kevrekidis, Clarence W Rowley, and M Williams, *A kernel-based method for data-driven koopman spectral analysis*, Journal of Computational Dynamics **2** (2016), no. 2, 247–265.
- [36] Bernard O Koopman, *Hamiltonian systems and transformation in hilbert space*, Proceedings of the National Academy of Sciences **17** (1931), no. 5, 315–318.
- [37] J Nathan Kutz, Steven L Brunton, Bingni W Brunton, and Joshua L Proctor, *Dynamic mode decomposition: data-driven modeling of complex systems*, SIAM, 2016.
- [38] Yueheng Lan and Igor Mezić, *Linearization in the large of nonlinear systems and koopman operator spectrum*, Physica D: Nonlinear Phenomena **242** (2013), no. 1, 42–53.
- [39] Yann LeCun, *Phd thesis: Modeles connexionnistes de l'apprentissage (connectionist learning models)*, (1987).
- [40] Kookjin Lee and Kevin T Carlberg, *Model reduction of dynamical systems on nonlinear manifolds using deep convolutional autoencoders*, Journal of Computational Physics **404** (2020), 108973.
- [41] Qianxiao Li, Felix Dietrich, Erik M Bollt, and Ioannis G Kevrekidis, *Extended dynamic mode decomposition with dictionary learning: A data-driven adaptive spectral decomposition of the koopman operator*, Chaos: An Interdisciplinary Journal of Nonlinear Science **27** (2017), no. 10, 103111.
- [42] Michel Loeve, *Probability theory: foundations, random sequences*, New York, NY: Van Nostrand, 1955.
- [43] Edward N Lorenz, *Empirical orthogonal functions and statistical weather prediction*, vol. 1, Massachusetts Institute of Technology, Department of Meteorology Cambridge, 1956.
- [44] David J Lucia, Philip S Beran, and Walter A Silva, *Reduced-order modeling: new approaches for computational physics*, Progress in aerospace sciences **40** (2004), no. 1-2, 51–117.

- [45] Zhengming Ma, Zengrong Zhan, Zijian Feng, and Jiajing Guo, *Manifold learning based on straight-like geodesics and local coordinates*, IEEE Transactions on Neural Networks and Learning Systems **32** (2020), no. 11, 4956–4970.
- [46] Igor Mezić, *Spectral properties of dynamical systems, model reduction and decompositions*, Nonlinear Dynamics **41** (2005), no. 1, 309–325.
- [47] ———, *Analysis of fluid flows via spectral properties of the koopman operator*, Annual review of fluid mechanics **45** (2013), 357–378.
- [48] ———, *Spectrum of the koopman operator, spectral expansions in functional spaces, and state-space geometry*, Journal of Nonlinear Science **30** (2020), no. 5, 2091–2145.
- [49] Igor Mezić and Andrzej Banaszuk, *Comparison of systems with complex behavior*, Physica D: Nonlinear Phenomena **197** (2004), no. 1-2, 101–133.
- [50] Hariharan Narayanan and Sanjoy Mitter, *Sample complexity of testing the manifold hypothesis*, Advances in neural information processing systems **23** (2010).
- [51] Pranshu Pant, Ruchit Doshi, Pranav Bahl, and Amir Barati Farimani, *Deep learning for reduced order modelling and efficient temporal evolution of fluid simulations*, Physics of Fluids **33** (2021), no. 10, 107101.
- [52] Sam T Roweis and Lawrence K Saul, *Nonlinear dimensionality reduction by locally linear embedding*, science **290** (2000), no. 5500, 2323–2326.
- [53] Clarence W Rowley, Igor Mezić, Shervin Bagheri, Philipp Schlatter, and Dan S Henningson, *Spectral analysis of nonlinear flows*, Journal of fluid mechanics **641** (2009), 115–127.
- [54] David Ruelle and Floris Takens, *On the nature of turbulence*, Les rencontres physiciens-mathématiciens de Strasbourg-RCP25 **12** (1971), 1–44.
- [55] Omer San and Romit Maulik, *Neural network closures for nonlinear model order reduction*, Advances in Computational Mathematics **44** (2018), 1717–1750.
- [56] Peter J Schmid, *Dynamic mode decomposition of numerical and experimental data*, Journal of fluid mechanics **656** (2010), 5–28.
- [57] Peter J Schmid, Larry Li, Matthew P Juniper, and O Pust, *Applications of the dynamic mode decomposition*, Theoretical and computational fluid dynamics **25** (2011), 249–259.
- [58] Arkadiy B Skopenkov, *Embedding and knotting of manifolds in euclidean spaces*, London Mathematical Society Lecture Note Series **347** (2008), 248.
- [59] Kunihiro Taira, Steven L Brunton, Scott TM Dawson, Clarence W Rowley, Tim Colonius, Beverley J McKeon, Oliver T Schmidt, Stanislav Gordeyev, Vassilios Theofilis, and Lawrence S Ukeiley, *Modal analysis of fluid flows: An overview*, Aiaa Journal **55** (2017), no. 12, 4013–4041.
- [60] Floris Takens, *Detecting strange attractors in turbulence*, Dynamical Systems and Turbulence, Warwick 1980: proceedings of a symposium held at the University of Warwick 1979/80, Springer, 2006, pp. 366–381.
- [61] Joshua B Tenenbaum, Vin de Silva, and John C Langford, *A global geometric framework for nonlinear dimensionality reduction*, science **290** (2000), no. 5500, 2319–2323.
- [62] Ioana Triandaf and Ira B Schwartz, *Karhunen-loeve mode control of chaos in a reaction-diffusion process*, Physical Review E **56** (1997), no. 1, 204.
- [63] Rui Wang, Xiao-Jun Wu, and Josef Kittler, *Symmet: A simple symmetric positive definite manifold deep learning method for image set classification*, IEEE Transactions on Neural Networks and Learning Systems **33** (2021), no. 5, 2208–2222.
- [64] Matthew O Williams, Ioannis G Kevrekidis, and Clarence W Rowley, *A data-driven approximation of the koopman operator: Extending dynamic mode decomposition*, Journal of Nonlinear Science **25** (2015), 1307–1346.
- [65] Junhai Zhai, Sufang Zhang, Junfen Chen, and Qiang He, *Autoencoder and its various variants*, 2018 IEEE international conference on systems, man, and cybernetics (SMC), IEEE, 2018, pp. 415–419.

CENTER FOR COMPLEX SYSTEMS SCIENCE, CLARKSON UNIVERSITY, POTSDAM, NY 13699-5815
 Email address: neranjaka.jayarathne@ieee.org

DEPARTMENT OF ELECTRICAL AND COMPUTER ENGINEERING AND THE CLARKSON CENTER FOR COMPLEX SYSTEMS SCIENCE, CLARKSON UNIVERSITY, POTSDAM, NEW YORK 13699, USA
 Email address: ebo11t@clarkson.edu